



BONE DENSITY GROWTH. BIOMECHANICS OF HEALTHY AND PROSTHETIC FEMUR AFTER A TOTAL HIP ARTHROPLASTY

Joan O'Connor

Lavinia Maria Alves Borges

Fernando Pereira Duda

Antonio Guilherme Barbosa da Cruz

joan@mecsol.ufrj.br

lavinia@mecanica.ufrj.br

duda@mecanica.coppe.ufrj.br

aguicruz@mecanica.coppe.ufrj.br

Programa de Engenharia Mecânica/COPPE, Universidade Federal do Rio de Janeiro,

Cidade Universitária, Rio de Janeiro, Brazil

Abstract. *The necessity of computational tools to predict the long-term behavior of bone implants and prosthetic devices in orthopedics, has a tremendous importance, considering population aging as a world wide problem. However, specifically in the hip prosthesis research area, the bone density growth process modeling using the finite element method (FEM) is still a challenging task. In this work, we investigate the bone density growth based on growth and remodeling theories for biological materials and its treatment using continuum mechanics. There are presented the kinematics, the balance laws for mass and linear momentum and the constitutive equations for bone density growth, along with the governing equations resulting from the coupling of the mass and momentum balances. We present an example considering the healthy and the prosthetic femur submitted to loads and bone formed by cortical and spongy tissues, which was carried out using daily physical activities load cases, for locate possible growth and resorption. In addition, a preliminary density growth model to locate bone growth or reabsorption zones for the intact femur and its post-operative condition is presented.*

Keywords: *Bone tissue, Density growth, Continuum mechanics, Finite elements*

1 INTRODUCTION

Total Hip Arthroplasties (THA) implantations associated to degenerative and traumatic hip conditions such as osteoarthritis, post-traumatic arthritis, and hip fractures, reaches about 500000 procedures performed annually in the UK and the USA, and are estimated in more than one million worldwide (Frenzel et al., 2015; Taylor and Prendergast, 2015; Pivec et al., 2012). Despite THA shows excellent clinical outcomes and is considered a successful and cost-effective procedure to relieve pain and restoring hip joint (Pivec et al., 2012), some prosthesis fails, most commonly due to aseptic loosening secondary to wear or dislocation (Smith et al., 2012; Malak et al., 2014). Therefore, the development of computational assessment tools with the capability to estimate bone growth and resorption when prosthetic devices are used has a remarkable importance, since these processes could determine the implant success or failure. In this scenario, the FEM has been playing a key role, being used to study and evaluate the mechanical behavior of prosthetic devices (Taylor and Prendergast, 2015; Prendergast, 1997), and to improve our understanding on the fundamentals of the mechanics of biological processes such as growth and remodeling (Taber, 1995; Ambrosi et al., 2011; Jones and Chapman, 2012; Menzel and Kuhl, 2012). Through the multiplicative decomposition of the deformation gradient, the biological growth is associated with soft tissues and remodeling with hard tissues, while the former are treated kinematically, considering changes in volume at constant density (Rodriguez et al., 1994; Kuhl, 2014; Menzel and Kuhl, 2012; Ambrosi et al., 2011), the latter are associated with changes in properties at constant volume (Taber, 1995; Ambrosi et al., 2011; Jones and Chapman, 2012; Menzel and Kuhl, 2012), such as internal structure, strength or density (Taber, 1995). In density growth case, focus of this work, the approach is of a constitutive kind using continuum nonlinear mechanics for hard tissues (Ambrosi et al., 2011; Menzel and Kuhl, 2012).

The objective of this work is the presentation of a density growth model theory, follow by the FEM implementation of a preliminary model to simulates for a healthy femur and for the femur with an implanted prosthesis (THA), submitted to loads equivalent to daily physical activities, based on growth and remodeling theories for biological materials. A model considering the effect of daily physical activities for healthy and for a prosthetic femur is also presented. We adopted a nonlinear formulation for large deformations using the isotropic functional adaptation approach proposed by (Harrigan and Hamilton, 1993), used for bone density growth applications (Kuhl and Steinmann, 2003b; Pang et al., 2012; Waffenschmidt et al., 2012).

2 THEORETICAL FRAMEWORK

Let consider a body \mathcal{B} capable of changing its density due to a mechanical stimulus, where two coupled processes are taking place: a mechanical one, driven by the body deformation due to loads and a biological one, related to density changes in an energy-driven format due to a mass source.

Body motion is given by the vector field χ , consequently, $\mathbf{v} = \dot{\chi}$ is the velocity field. Mapping $\mathbf{x} = \chi(\mathbf{X}, t)$ is considered one-to-one in \mathbf{X} for fixed t , so invertible then: $\mathbf{X} = \chi^{-1}(\mathbf{x}, t)$, being \mathbf{X} and \mathbf{x} , the position vectors referred to reference and current configurations. Deformation gradient is defined as $\mathbf{F} = \nabla\chi$ and the volumetric Jacobian of the deformation is the determinant of \mathbf{F} , being: $J = \det(\mathbf{F})$. Dot symbol and ∇ operator denote material time derivative and gradient of a quantity. The displacement \mathbf{u} of \mathbf{X} is defined as $\mathbf{u}(\mathbf{X}, t) = \chi(\mathbf{X}, t) - \mathbf{X}$,

where its gradient is related with \mathbf{F} through $\mathbf{F} = \mathbf{I} + \nabla\mathbf{u}$, being \mathbf{I} the second-order identity tensor. Density growth process is regulated by the rate of the density scalar field ρ_K .

2.1 Balance equations

In the mass balance¹, the rate change of mass due to volumetric mass sources, neglecting mass fluxes (Kuhl et al., 2003; Pang et al., 2012; Waffenschmidt et al., 2012), is given by:

$$\dot{\rho}_K = \Gamma_K \quad (1)$$

expressing the equilibrium of the rate change of mass $\dot{\rho}_K$ with the mass source Γ_K , being ρ_K the mass density.

The linear momentum balance, balances the rate change of momentum $\overline{\rho_K \mathbf{v}}$ with the momentum contributions of traction, body forces and mass source (Kuhl and Steinmann, 2003a; Epstein and Maugin, 2000; Lubarda and Hoger, 2002), hence:

$$\overline{\rho_K \dot{\mathbf{v}}} = \text{Div} \mathbf{P} + \mathbf{b} + \Gamma_K \mathbf{v} \quad (2)$$

being \mathbf{v} the velocity, \mathbf{b} the body force and \mathbf{P} the first Piola-Kirchhoff stress tensor. Div denotes the divergence of a quantity. Considering (1) in (2), the linear momentum balance gives:

$$\rho_K \dot{\mathbf{v}} = \text{Div} \mathbf{P} + \mathbf{b} \quad (3)$$

2.2 Density growth constitutive equations

In the mass balance of (1), the mass source term Γ_K has the following form (Harrigan and Hamilton, 1993):

$$\Gamma_K = c \left(\left[\frac{\rho_K}{\rho_{K^*}} \right]^{-m} \psi_K - \psi_{K^*} \right) \quad (4)$$

being ρ_{K^*} the initial density, ψ_{K^*} the stimulus attractor (Carter and Beaupré, 2007), considered as the energy saturation value for density evolution (Waffenschmidt et al., 2012), m the bone adaptation process exponent (Harrigan and Hamilton, 1993), and c the adaptation process coefficient (Kuhl et al., 2003), assumed equals to unity. The strain energy density form adopted is:

$$\psi_K = \left[\frac{\rho_K}{\rho_{K^*}} \right]^n \psi_K^{neo} \quad (5)$$

with the relative density term $[\rho_K/\rho_{K^*}]^n$ used for open-pored cell materials (Carter and Hayes, 1977; Gibson and Ashby, 1982), where n is the porosity exponent.

By neglecting tissues viscous effects for short time-scales (seconds or minutes order) and assuming that growth occurs for large time-scales (weeks or months), its constitutive response can be considered as hyperelastic (Kuhl and Steinmann, 2003b). Accordingly, the strain energy function considered is of a Neo-Hookean type (Attard, 2003):

$$\psi_K^{neo} = \left[\frac{\lambda}{2} \ln^2 J + \frac{\mu}{2} \left(\mathbf{F}^T \mathbf{F} : \mathbf{I} - 3 - 2 \ln J \right) \right] \quad (6)$$

being λ and μ the Lamé constants and \mathbf{F}^T the transpose of \mathbf{F} .

¹Mass and momentum balances are presented in the local form referred to the reference configuration.

Piola-Kirchhoff Stress can be obtained through the derivative of the strain energy with respect to the deformation gradient, hence, using (5) and (6):

$$\mathbf{P} = \frac{\partial \psi_K}{\partial \mathbf{F}} = \left[\frac{\rho_K}{\rho_{K^*}} \right]^n [(\lambda \ln J - \mu) \mathbf{F}^{-T} + \mu \mathbf{F}] \quad (7)$$

being \mathbf{F}^{-T} the inverse of the transpose of \mathbf{F} .

3 GOVERNING EQUATIONS AND BOUNDARY CONDITIONS FOR DENSITY GROWTH

The governing equations are obtained coupling the biological problem, defined through the mass balance, with the mechanical problem defined through the momentum balance, hence:

$$\dot{\rho}_K = \frac{1}{2} \left[\frac{\rho_K}{\rho_{K^*}} \right]^{n-m} [\lambda \ln^2 (J) + \mu [\mathbf{F}^T \mathbf{F} : \mathbf{I} - 3 - 2 \ln (J)]] - \psi_K^* \quad (8)$$

$$\mathbf{0} = \text{Div} \left(\left[\frac{\rho_K}{\rho_{K^*}} \right]^n [(\lambda \ln J - \mu) \mathbf{F}^{-T} + \mu \mathbf{F}] \right) \quad (9)$$

considering a quasi-static process and neglecting body forces.

The boundary conditions that supplement the above governing equations can be established as follows: Let the body \mathcal{B} be given with loading surface tractions $\bar{\tau}$ defined on $\partial_\tau \mathcal{B}$, and with prescribed displacements $\bar{\mathbf{u}} = 0$ on $\partial_u \mathcal{B}$, then, Neumann and Dirichlet boundary conditions (BC) for the mechanical problem are, respectively

$$\begin{aligned} \mathbf{P}(\mathbf{X})\mathbf{n}(\mathbf{X}) &= \bar{\tau}(\mathbf{X}), & \mathbf{X} &\in \partial_\tau \mathcal{B} \\ \mathbf{u}(\mathbf{X}) &= \bar{\mathbf{u}}(\mathbf{X}), & \mathbf{X} &\in \partial_u \mathcal{B} \end{aligned} \quad (10)$$

where \mathbf{n} is the unit normal to $\partial_\tau \mathcal{B}$. Prescribed displacements $\bar{\mathbf{u}}$ and prescribed tractions $\bar{\tau}$ are given functions on $\partial_u \mathcal{B}$ and $\partial_\tau \mathcal{B}$ which are respectively, complementary disjoints of $\partial \mathcal{B}$. Within the mechanical problem is embedded the biological density growth boundary value problem given by the mass balance (1), with the initial condition:

$$\rho_K(\mathbf{X}, 0) = \rho_{K^*} \quad (11)$$

4 NUMERICAL APPLICATION

To solve the theoretical model presented, we have used COMSOL Multiphysics v 4.4. The goal is to solve the incremental problem of density evolution due to the mass source Γ_K for an hyperelastic material, embedded into the mechanical problem, which is coupled to density through the deformation field generated in response to the applied load. The coupled problem given by the nonlinear system equations formed by (8) and (9), was solved numerically using the Solid Mechanics mode for the mechanical problem, and using the General Form PDE for the biological problem of density evolution. The strain energy function was reprogrammed including the relative density term in the Neo-Hookean hyperelastic strain energy. A function for the mass source term Γ_K was also implemented.

The model was discretized with Lagrangian² quadratic elements to interpolate displacements \mathbf{u} and the density ρ_K . For the time discretization, a General- α backward differentiation method was used (Chung and Hulbert, 1993). The MUMPS (MUMPS, 1996) solver was used to solve the discrete system resulting from each time step discretization with residual tolerance levels of 10^{-4} , which is considered sufficient since similar solutions were obtained at lower tolerance levels. Plane stress condition was adopted.

5 GEOMETRICAL MODEL

The geometrical two-dimensional (2D) model for healthy femur (HF) and for the femur with an implanted prosthesis (FP) is shown in Fig. 1 corresponding to a 2D slice in the mid-frontal plane for healthy and prosthetic femur.

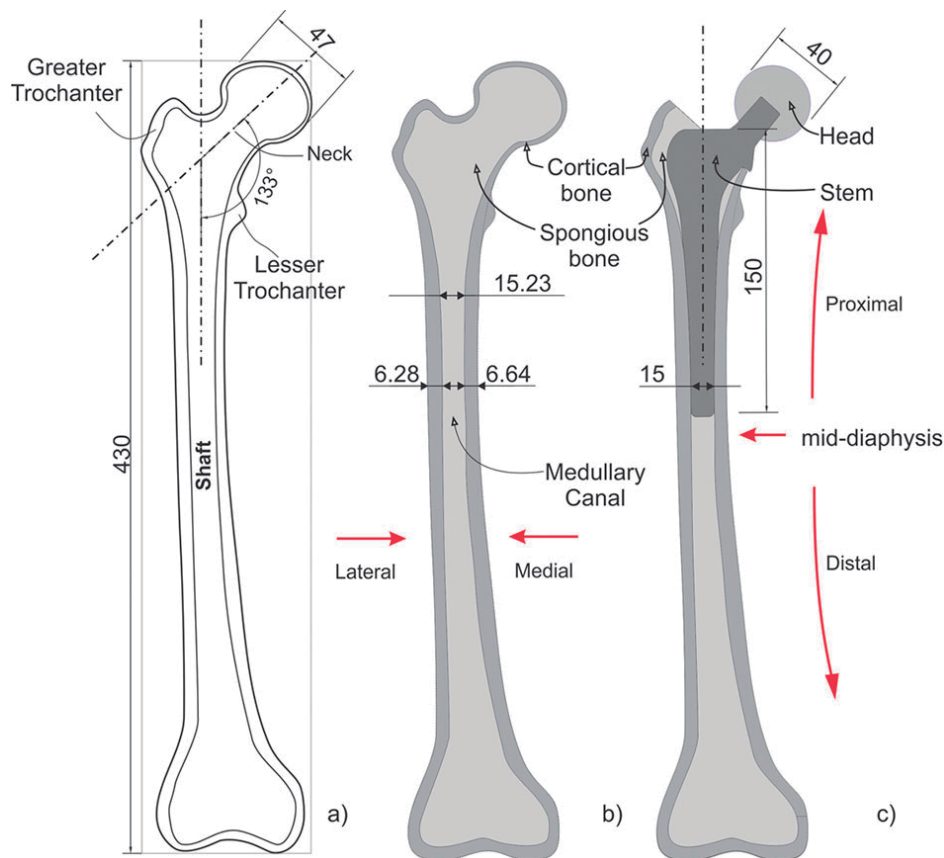


Figure 1: Two-dimensional geometrical model of HF and FP, relevant dimensions, characteristics and main anatomical landmarks. a) HF: total length, neck-shaft angle and head diameter. b) HF 2D model: medullary canal diameter and cortical wall thickness at the mid-diaphysis (by medial and lateral). c) FP 2D model: prosthesis stem length and size (diameter) and head diameter. (All dimensions are in millimeters)

Cortical and spongy tissues contours were obtained in previous works (O'Connor et al., 2011), and compared with femur anatomical standard dimensions of a human adult (Husmann et al., 1997). Tissues contours Splines were converted to 2D surfaces to generate cortical and

²Lagrangian quadratic: $Lag_k(T)$, $k = 2$, being k the polynomial degree of the element shape function and T the mesh type: triangular in this case (COMSOL, 2013)

spongy domains. The prosthesis is considered as conceptual (cementless type), with typical dimensions according to specialized literature (Chandran et al., 2010; Gabbar et al., 2008). The tissues and prosthesis (stem and head) geometrical domains were generated using software Solidworks version 2013 and a coupled structure-structure model was constructed using boolean operations in COMSOL Multiphysics.

6 RESULTS AND DISCUSSION

6.1 Example 1: Dynamic model without considering density growth

Firstly, it was implemented a FEM model without considering density growth for HF and FP, submitted to three daily physical activities: Normal walk (NW), going up stairs (US) and going down stairs (DS), to locate high-stress concentration zones that could be possible density growth areas. Loads conditions and model meshes are shown in Fig. 2. Zero displacements BC were considered in femurs distal ends (Fig. 2a.1). Loads were applied on HF and FP heads (Fig. 2a). Load functions were taken from public database Orthoload (Bergmann, 2009), considering x and y components for the three load cases (Fig. 2a.2). Abductor muscle force was considered of 703 N applied on the greater trochanter (Kuhl and Balle, 2005; Carter and Beaupré, 2007).

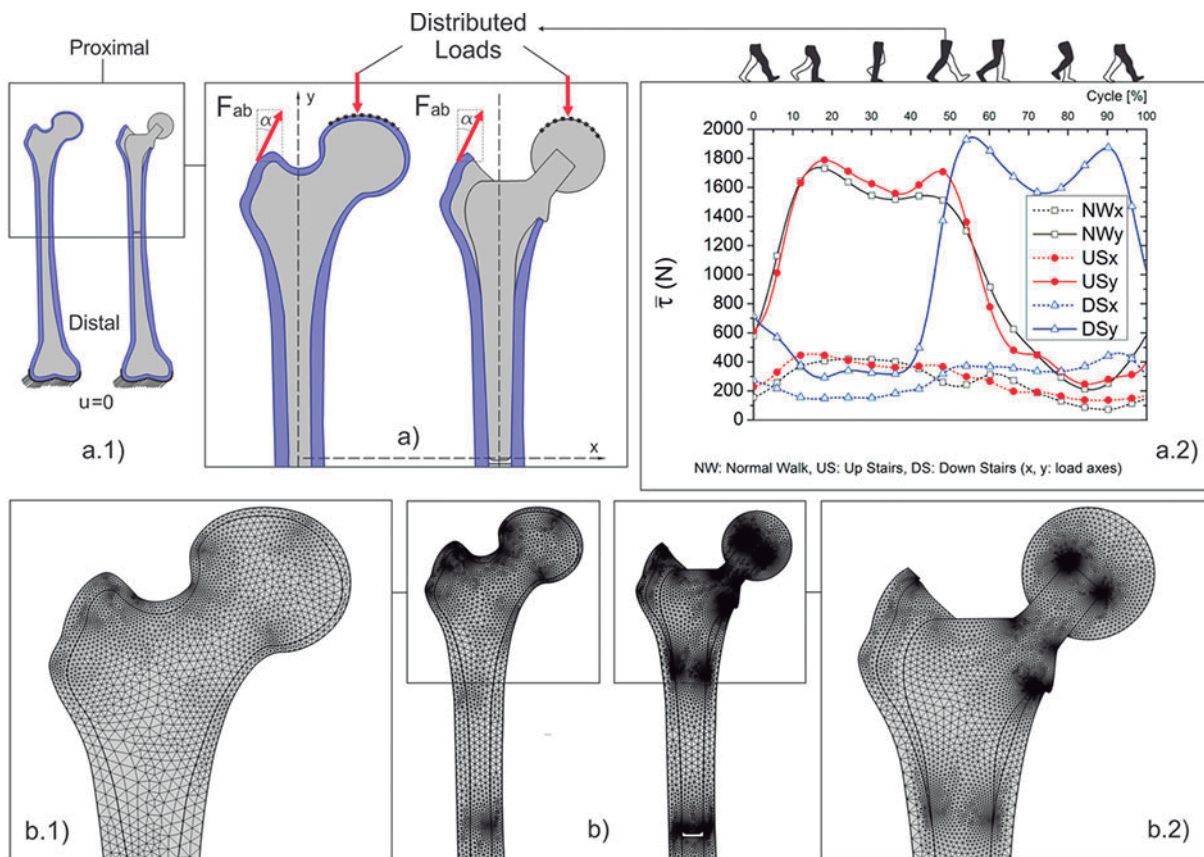


Figure 2: Loads, boundary conditions, and meshes for HF and for FP. a) Proximal part of the model domains, applied load regions for daily activities loads and abductor forces (F_{ab}), with $\alpha = 28^\circ$. a.1) Dirichlet BC of zero displacements in HF and FP distal ends. a.2) Daily activities loads values for: NW, US and DS. Load functions values were taken from public database Orthoload (Bergmann, 2009), with permission. b) Meshes of HF and FP proximally. b.1), b.2) Meshes details.

Table 1: Material properties for cortical and spongy tissues and for prosthesis biomaterials

	E	ν	λ	μ	ρ	σ_{yc}	σ_{yt}
	(MPa)		(MPa)	(MPa)	(kg/m ³)	(MPa)	(MPa)
Cortical bone	16000	0.3	9230	6153	1800	115	121
Spongy bone	2000	0.3	1153	769	600		
Ti6Al4V alloy	110000	0.3	63461	42307		970	880
Co-Cr alloy	230000	0.3	132692	88461			

E, ν : Young modulus and Poisson ratio. σ_{yc} , σ_{yt} : Compressive and tensile yield strength

Cortical and spongy tissues were considered as hyperelastic, homogeneous and isotropic (Kuhl and Balle, 2005; Cowin and Doty, 2007; Goldstein, 1987) and prosthesis materials, as linear elastics and isotropic, using a Titanium alloy and a Cobalt-Chromium alloy for stem and head, respectively (Niinomi and Nakai, 2011; Wong and Bronzino, 2007), material properties are shown in Table 1. The model was discretized in 27712 elements (Fig. 2b), and solved for 118914 degrees of freedom (DOF), after two previous mesh refinement steps until convergence was achieved. The total time for simulations were: $t_{NW} = 1.103$ s, $t_{US} = 1.593$ s and $t_{DS} = 1.439$ s, corresponding to 100% of the entire cycle of each load case (Bergmann, 2009). The time step used was $\Delta t = 0.01$. Bone-prosthesis interface was considered as fully bonded (Jonkers et al., 2008; Bougherara et al., 2010).

6.2 Dynamic model results

The interest of this work is focus in cortical bone tissue since it is the main responsible for prosthesis stem fixation. However, some results concerning prosthesis will briefly discuss. Results were analyzed and there were found three main critical regions, coincident in location for the three load cases. Region 1: located in medial cortical wall HF mid-diaphysis, region 2: in medial cortical wall FP mid-diaphysis, and region 3: in HF neck as shown in Fig. 3, where it can be found the Von Mises stress distribution of analyzed load cases at times: $t_{NW} = 0.55$ s, $t_{US} = 0.81$ s and $t_{DS} = 0.8$ s, for a NW, US and DS respectively, where maximum stresses were attained. Additionally, a region 4 located in FP neck, was included in the analysis to compare critical regions for both situations, healthy and post-operative.

Higher stresses were found in HF over the medial cortical wall from mid-diaphysis to proximal for NW due to a higher bending moment, when compared with US and DS, where a predominant compressive situation leads to stresses concentration in the neck, also is observed, that the higher stresses were located in femurs necks for the healthy condition for the three load cases (Fig. 3a-c). In contrast, in FP, the higher stresses were found in mid-diaphysis, being the most critical situation for NW, due to a higher bending moment (Fig. 3d-f). In FP neck, an unloading situation was detected proximally due to stress shielding, being critical for US.

There are also plotted the stresses along HF and FP medial inner and outer cortical walls (Fig. 3 right panels), from a point **p** located proximally in femurs necks (at lesser trochanter height) to a point **d** located in the mid-diaphysis. As shown in Fig. 3, stresses were higher in FP medial cortical wall mid-diaphysis (region 2) than in HF analogous region for the three

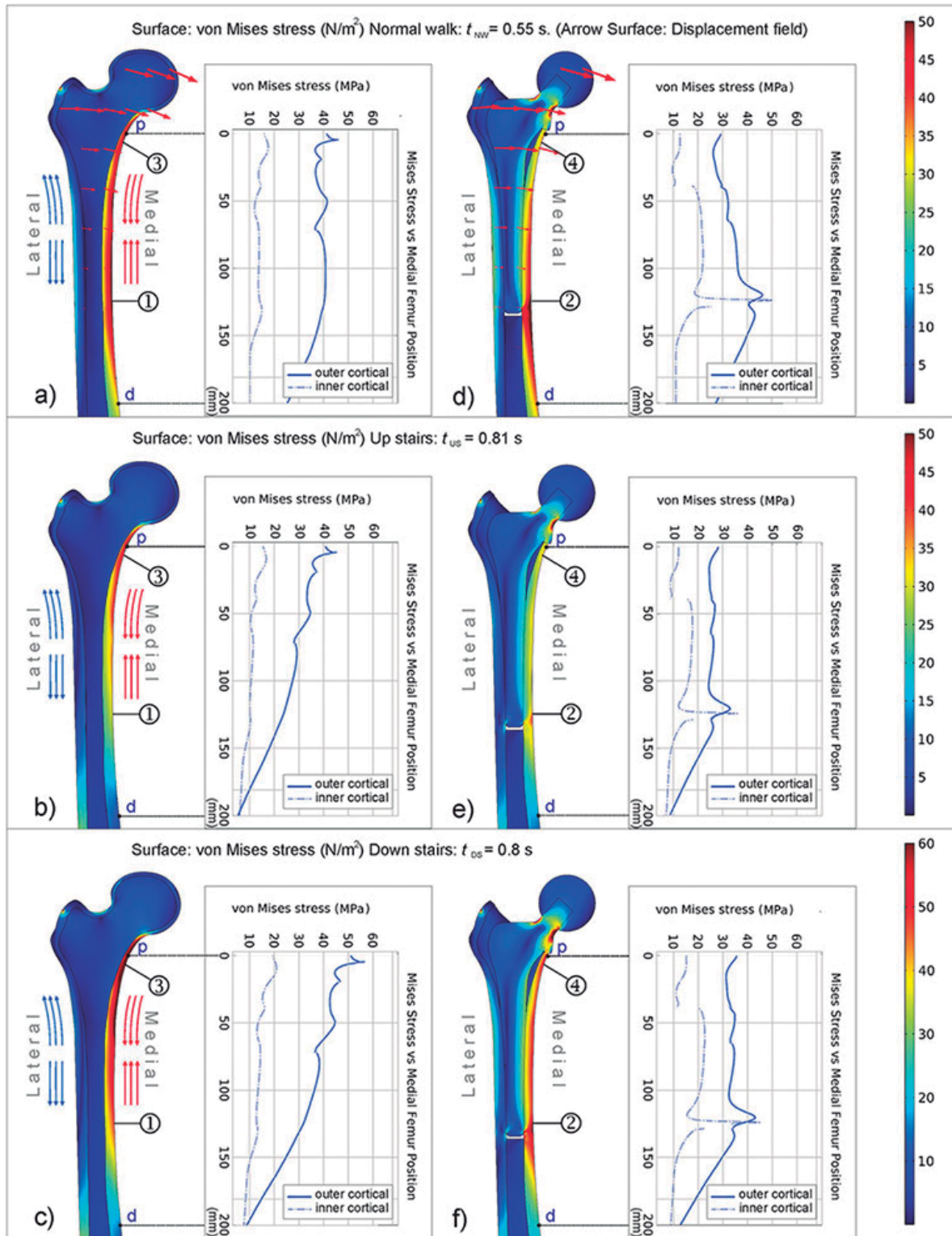


Figure 3: Von Mises stress distribution at physical activities times where maximum stresses were attained, critical regions, and stresses along medial cortical walls from proximal to distal (outer and inner cortical stresses from point p to point d), in HF (left) and FP (right) for: a, d) NW at $t = 0.55$ s (the red arrows describes the displacements vector field); b, e) US at $t = 0.81$ s; c, f) DS at $t = 0.8$ s. Being 1, 2, 3 and 4, the critical regions.

load cases, indicating that for a prosthetic condition, bone is significantly overloading (in about 10 MPa), in the outer cortical wall due to a bending moment and at inner cortical wall due to the prosthesis distal tip load transferring contribution. We hypothesized that these critical areas (Fig. 3d-f), could be one of the causes of periprosthetic fractures that commonly occurs underneath of implanted prosthesis (Frenzel et al., 2015; Fleischman and Chen, 2015; Drexler et al., 2014).

Regarding FP neck (region 4, Fig. 3d-f), stresses were lower (in about 17 MPa) than in the analogous HF region for the three load cases due to the unloading situation proximally. It was also significant that stresses over FP medial cortical wall were higher and more uniformly distributed (through the cortical thickness) for DS than for NW and US activities (Fig. 3d-f), suggesting that DS activity may stimulate bone in the medial cortical wall and may reduce the unloading situation in FP proximally. Maximum stresses (Fig. 3) were below cortical bone compressive and tensile yield strength values (Table 1), without compromise bone integrity. In the prosthesis, most significative stresses were found in the neck between 70 and 97 MPa (Fig. 3d-f), in agreement with (Bougherara et al., 2010), reporting values between 85 and 75 MPa. Stresses obtained, were below the titanium alloy compressive and tensile yield strength (Table 1). Even though a fatigue analysis is required, however, fatigue is out the scope of the current work.

In addition, four probes were positioned in the regions of interest to analyze stresses and strains behavior through the time for the three load cases (not presented in the paper). From the analysis of intervals: 10 - 50% NW, 15 - 55% US and 50 - 90% DS, stresses were significantly higher in FP region 2 than in HF region 1 all over the referred intervals, confirming, that bone in the mid-diaphysis is submitted to higher stresses levels post-operatively (7 - 10 MPa overloaded), being NW activity, the most critical situation. Regarding femoral neck, for prosthetic condition (region 4), stresses were significantly lower than for healthy condition (region 3), confirming the unloading situation (of about 13 - 17 MPa), found previously. Maximum stresses and strains found at: 50% NW, 52% US and 53% DS, are shown in Table 2.

This part of the study has examined the biomechanical behavior of healthy femur and its post-operative condition after a THA surgery for three daily physical activities. From a qualitative point of view, there were found higher stresses in compressed cortical wall medially than in tensed cortical wall laterally, in agreement with (Wagner et al., 2010; Jonkers et al., 2008). Also, Von Mises stress results reproduced the typical bending stress distribution reported in literature with maximum values located in mid-diaphysis medial cortical bone for healthy and prosthetic condition (Piao et al., 2014; Wagner et al., 2010; Jonkers et al., 2008). However, direct comparisons with other authors reports are often difficult, due to the load levels variability in numerical and experimental studies and material properties and boundary conditions adopted in numerical studies.

6.3 Example 2: Density growth model

In this example is implemented a preliminary density growth FEM model for HF and FP submitted to loads equivalent to the physical activities studied previously, following the formulation presented in sections 2 and 3, in order to analyze bone growth and resorption in the regions of interest for the healthy and post-operative femur condition.

A multiple step load type was considered (Kuhl and Steinmann, 2003b; Waffenschmidt

Table 2: Maximum stresses and strains in HF and FP critical regions at 50% NW, 52% US and 53% DS of physical activities

	Stress (MPa)			Strain ($\mu\epsilon$)		
	NW(50%)	US(52%)	DS(53%)	NW(50%)	US(52%)	DS(53%)
HF 1	40.36	24.00	33.00	1120	677	906
FP 2	46.00	32.80	43.14	1250	899	1180
HF 3	42.50	41.17	52.00	1117	1180	1430
FP 4	29.00	28.00	35.40	800	788	972

$\mu\epsilon$: microstrains

et al., 2012), acting on HF and FP as an average daily load, in a range of a NW. The multiple step load was considered of 1850 N, applied in femur and prosthesis heads as shown in Fig. 4a (250 N increment was added to include DS load levels). Cortical and spongy tissues were treated as hyperelastic, homogeneous and isotropic.

The corresponding density variables were defined as ρ_{Kc} and ρ_{Ke} and computed using the density evolution expression from the governing equations of section 3. The corresponding mass sources Γ_{Kc} and Γ_{Ke} , were implemented (see section 2.2). Initial density was $\rho_K^* = 600 \text{ kg/m}^3$ for both tissues, under homogeneous density assumption at simulation start. The stimulus attractor considered was $\psi_K^* = 0.01 \text{ MPa}$ according to (Carter and Beaupré, 2007; Kuhl and Balle, 2005; Kuhl et al., 2003; Kuhl and Steinmann, 2003b) and the parameters values were $n = 2$, $m = 3$ (Waffenschmidt et al., 2012; Kuhl and Balle, 2005; Kuhl et al., 2003; Kuhl and Steinmann, 2003b). Prosthesis materials were treated as in the previous example (Table 1). Also, the previous example model mesh was adopted (Fig. 2b). Simulation total time was $t = 40$ dimensionless time units, and the time step for the incremental problem was $\Delta t = 0.01$.

6.4 Density growth model results

In this work is only analyzed the density behavior in the regions of interest found in the previous example. Density evolution in these regions was measured over time (Fig. 4b), exhibiting a relaxation tendency to biological equilibrium, where each load increases is followed by changes in density towards to a new equilibrium state for the loading history $\bar{\tau}$, as obtained in (Kuhl and Steinmann, 2003a,b; Waffenschmidt et al., 2012).

An increase of density in high-stress concentration areas and a bone resorption situation associated to low-stress regions were obtained, consistent with (Kuhl and Balle, 2005; Jonkers et al., 2008; Avval et al., 2015), also this phenomenon was confirmed since localization of significative growth and resorption regions coincide with critical stresses regions found in the previous example. At simulations end, density values obtained for HF, were in agreement with values reported by (Ashman and Rho, 1988; Natali and Meroi, 1989).

The nonlinear behavior and relaxation behavior of density towards to biological equilibrium is observed in Fig. 4b. Each load increase of $\bar{\tau}$ is followed by changes in density converging to a new equilibrium state, where biological stimulus equals the attractor ψ_K^* , mass source Γ_{Kc} vanishes and ρ_{Kc} undergoes no further changes in cortical tissue, providing to HF and FP

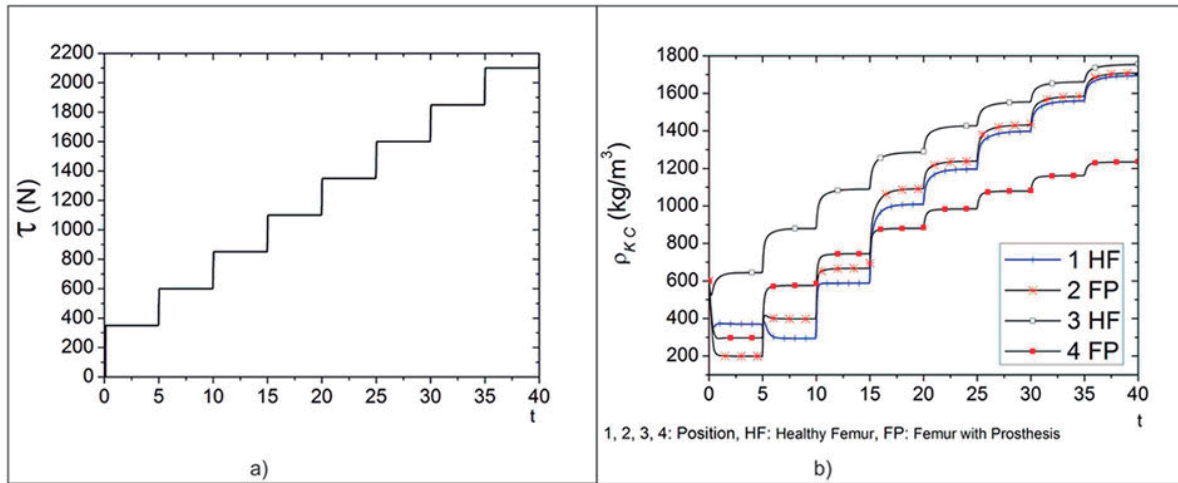


Figure 4: Density prediction for HF and FP, multiple step load and density evolution in the regions of interest. a) Multiple step load. b) Density evolution (where 1, 2, 3 and 4 are the regions of interest).

the optimal density distributions to support the load environment simulated, in agreement with (Kuhl and Steinmann, 2003b; Waffenschmidt et al., 2012; Pang et al., 2012).

Finally, the proposed model results analysis is in a preliminary research stage. However, density growth results shown good agreement with previous results presented by other authors and the model is shown promissory.

7 CONCLUSIONS

A density growth model for hard tissues based on growth and remodeling theories was presented in this work and was implemented in a FEM software.

For the model considering physical activities, results shown that for post-operative condition: (i) Bone is significantly overloading in the mid-diaphysis, situation that may lead to peri-prosthetic fractures. (ii) Going down stairs activity is suggested to stimulate bone and to reduce the unloading situation detected proximally.

For the density growth model implemented, preliminary results obtained for bone density evolution due to loads are in agreement with literature.

The proposed density growth model in conjunction with the dynamical model for daily physical activities loads, represents a potentially computational assessment tool for orthopedic surgeons, to evaluate the behavior of the healthy femur and its post-operative condition after a THA procedure.

8 ACKNOWLEDGEMENTS

The authors gratefully acknowledge the financial support provided by CNPQ under grant (870068/1997.0) and CAPES PNP (31001017030D4)

Bibliography

- Ambrosi, D., Ateshian, G., Arruda, E., Cowin, S., Dumais, J., Goriely, A., Holzapfel, G., Humphrey, J., Kemkemer, R., Kuhl, E., Olberding, J., Taber, L., Garikipati, K., 2011. Perspectives on biological growth and remodeling. *Journal of the Mechanics and Physics of Solids* 59, 863 – 883.
- Ashman, R.B., Rho, J.Y., 1988. Elastic modulus of trabecular bone material. *Journal of Biomechanics* 21, 177–181.
- Attard, M.M., 2003. Finite strain isotropic hyperelasticity. *International Journal of Solids and Structures* 40, 4353 – 4378.
- Avval, P.T., Samiezadeh, S., Klika, V., Bougherara, H., 2015. Investigating stress shielding spanned by biomimetic polymer-composite vs. metallic hip stem: A computational study using mechano-biochemical model. *Journal of the Mechanical Behavior of Biomedical Materials* 41, 56 – 67.
- Bergmann, G., 2009. Orthoload. (ed.) Charité Universitaetsmedizin Berlin (2008). Retrieved Feb. 1, 2009 from <http://www.OrthoLoad.com>.
- Bougherara, H., Zdero, R., Shah, S., Miric, M., Papini, M., Zalzal, P., Schemitsch, E.H., 2010. A biomechanical assessment of modular and monoblock revision hip implants using fe analysis and strain gage measurements. *Journal of orthopaedic surgery and research* 5, 34.
- Carter, D., Beaupré, G., 2007. *Skeletal Function and Form: Mechanobiology of Skeletal Development, Aging, and Regeneration*. Cambridge University Press.
- Carter, D.R., Hayes, W.C., 1977. The compressive behavior of bone as a two-phase porous structure. *The Journal of Bone & Joint Surgery* 59, 954–962.
- Chandran, P., Azzabi, M., Miles, J., Andrews, M., Bradley, J., 2010. Furlong hydroxyapatite-coated hip prosthesis vs the charnley cemented hip prosthesis. *The Journal of Arthroplasty* 25, 52–57.
- Chung, J., Hulbert, G.M., 1993. A time integration algorithm for structural dynamics with improved numerical dissipation: The generalized- method. *Journal of Applied Mechanics* 60, 371 – 375.
- COMSOL, 2013. *Comsol multiphysics. Reference Manual. 2013 version 4.4*, Comsol .
- Cowin, S., Doty, S., 2007. *Tissue Mechanics*. Springer.
- Drexler, M., Dwyer, T., Chakraverty, R., Backstein, D., Gross, A.E., Safir, O., 2014. The out-

- come of modified extended trochanteric osteotomy in revision {THA} for vancouver b2/b3 periprosthetic fractures of the femur. *The Journal of Arthroplasty* 29, 1598 – 1604.
- Epstein, M., Maugin, G.A., 2000. Thermomechanics of volumetric growth in uniform bodies. *International Journal of Plasticity* 16, 951–978.
- Fleischman, A.N., Chen, A.F., 2015. Periprosthetic fractures around the femoral stem: overcoming challenges and avoiding pitfalls. *Annals of Translational Medicine* 3, 234.
- Frenzel, S., Vécsei, V., Negrin, L., 2015. Periprosthetic femoral fractures—incidence, classification problems and the proposal of a modified classification scheme. *International Orthopaedics* 39, 1909–1920.
- Gabbar, O.A., Rajan, R.A., Londhe, S., Hyde, I.D., 2008. Ten- to twelve-year follow-up of the furlong hydroxyapatite-coated femoral stem and threaded acetabular cup in patients younger than 65 years. *The Journal of Arthroplasty* 23, 413–417.
- Gibson, L.J., Ashby, M.F., 1982. The mechanics of three-dimensional cellular materials. *Proceedings of the Royal Society of London. A. Mathematical and Physical Sciences* 382, 43–59.
- Goldstein, S.A., 1987. The mechanical properties of trabecular bone: Dependence on anatomic location and function. *Journal of Biomechanics* 20, 1055–1061.
- Harrigan, T.P., Hamilton, J.J., 1993. Finite element simulation of adaptive bone remodelling: a stability criterion and a time stepping method. *International Journal for Numerical Methods in Engineering* 36, 837–854.
- Husmann, O., Rubin, P.J., Leyvraz, P.F., de Roguin, B., Argenson, J.N., 1997. Three-dimensional morphology of the proximal femur. *The Journal of Arthroplasty* 12, 444 – 450.
- Jones, G.W., Chapman, S.J., 2012. Modeling growth in biological materials. *SIAM Review* 54, 52–118.
- Jonkers, I., Sauwen, N., Lenaerts, G., Mulier, M., der Perre, G.V., Jaecques, S., 2008. Relation between subject-specific hip joint loading, stress distribution in the proximal femur and bone mineral density changes after total hip replacement. *Journal of Biomechanics* 41, 3405 – 3413.
- Kuhl, E., 2014. Growing matter: A review of growth in living systems. *Journal of the Mechanical Behavior of Biomedical Materials* 29, 529 –543.
- Kuhl, E., Balle, F., 2005. Computational modeling of hip replacement surgery: Total hip replacement vs. hip resurfacing. *Technische mechanik* 25, 107–114.
- Kuhl, E., Menzel, A., Steinmann, P., 2003. Computational modeling of growth. *Computational Mechanics* 32, 71–88.
- Kuhl, E., Steinmann, P., 2003a. Mass and volume specific views on thermodynamics for open systems. *Proceedings of the Royal Society of London. Series A Mathematical, Physical and Engineering Sciences* 459, 2547–2568.
- Kuhl, E., Steinmann, P., 2003b. Theory and numerics of geometrically non-linear open system mechanics. *International Journal for Numerical Methods in Engineering* 58, 1593–1615.

- Lubarda, V., Hoger, A., 2002. On the mechanics of solids with a growing mass. *International Journal of Solids and Structures* 39, 4627 – 4664.
- Malak, T.T., Beard, D., Glyn-Jones, S., 2014. Total hip arthroplasty: recent advances and controversies. *Topical Reviews Arthritis Research UK* , 1–8.
- Menzel, A., Kuhl, E., 2012. Frontiers in growth and remodeling. *Mechanics Research Communications* 42, 1 – 14.
- MUMPS, 1996. Multifrontal massively parallel sparse direct solver. <http://graal.ens-lyon.fr/MUMPS/> (MUMPS Consortium, accessed April 3, 2015).
- Natali, A.N., Meroi, E.A., 1989. A review of the biomechanical properties of bone as a material. *Journal of biomedical engineering* 11, 266–76.
- Niinomi, M., Nakai, M., 2011. Titanium-based biomaterials for preventing stress shielding between implant devices and bone. *International Journal of Biomaterials* 2011, 10.
- O'Connor, J., Rodriguez, M., Calas, H., Moreno, E., Palomares, E., 2011. Modelacion y simulacion de sistemas biomecanicos acoplados utilizando el metodo de elementos finitos. aplicaciones en ortopedia. *IFMBE Proceedings: V Latin American Congress on Biomedical Engineering CLAIB 2011. Habana, Cuba* 33, 619–622.
- Pang, H., Shiwalkar, A., Madormo, C., Taylor, R., Andriacchi, T., Kuhl, E., 2012. Computational modeling of bone density profiles in response to gait: a subject-specific approach. *Biomechanics and Modeling in Mechanobiology* 11, 379–390.
- Piao, C., Wu, D., Luo, M., Ma, H., 2014. Stress shielding effects of two prosthetic groups after total hip joint simulation replacement. *Journal of Orthopaedic Surgery and Research* 9, 1–8.
- Pivec, R., Johnson, A.J., Mears, S.C., Mont, M.A., 2012. Hip arthroplasty. *The Lancet* 380, 1768 – 1777.
- Prendergrast, P., 1997. Finite element models in tissue mechanics and orthopaedic implant design. *Clinical Biomechanics* 12, 343–366.
- Rodriguez, E., Hoger, A., McCulloch, D., 1994. Stress dependent finite growth in soft elastic tissues. *Journal of Biomechanics* 27, 445–467.
- Smith, A.J., Dieppe, P., Vernon, K., Porter, M., Blom, A.W., 2012. Failure rates of stemmed metal-on-metal hip replacements: analysis of data from the national joint registry of england and wales. *The Lancet* 379, 1199 – 1204.
- Taber, L.A., 1995. Biomechanics of growth, remodeling, and morphogenesis. *Applied Mechanics Reviews* 48, 487–545.
- Taylor, M., Prendergast, P.J., 2015. Four decades of finite element analysis of orthopaedic devices: Where are we now and what are the opportunities? *Journal of Biomechanics* 48, 767 – 778. In Memory of Rik Huiskes.
- Waffenschmidt, T., Menzel, A., Kuhl, E., 2012. Anisotropic density growth of bonea computational micro-sphere approach. *International Journal of Solids and Structures* 49, 1928 – 1946.

- Wagner, D.W., Divringi, K., Ozcan, C., Grujicic, M., Pandurangan, B., Grujicic, A., 2010. Combined musculoskeletal dynamics/structural finite element analysis of femur physiological loads during walking. *Multidiscipline Modeling in Materials and Structures* 6, 417–437.
- Wong, J., Bronzino, J., 2007. *Biomaterials*. Taylor & Francis.